

# Controlled buckling of semiconductor nanoribbons for stretchable electronics

YUGANG SUN<sup>1,2\*†</sup>, WON MOOK CHOI<sup>1</sup>, HANQING JIANG<sup>3</sup>, YONGGANG Y. HUANG<sup>3</sup>  
AND JOHN A. ROGERS<sup>1,3†</sup>

<sup>1</sup>Department of Materials Science and Engineering, Beckman Institute, and Seitz Materials Research Laboratory, University of Illinois at Urbana-Champaign, 1304 West Green Street, Urbana, Illinois 61801, USA

<sup>2</sup>Center for Nanoscale Materials, Argonne National Laboratory, 9700 South Cass Avenue, Argonne, Illinois 60439, USA

<sup>3</sup>Department of Mechanical and Industrial Engineering, University of Illinois at Urbana-Champaign, Urbana, Illinois 61801, USA

\*Present address: Argonne National Laboratory, 9700 South Cass Avenue, Argonne, Illinois 60439, USA

†e-mail: ygsun@anl.gov; jrogers@uiuc.edu

Published online: 5 December 2006; doi:10.1038/nnano.2006.131

Control over the composition, shape, spatial location and/or geometrical configuration of semiconductor nanostructures is important for nearly all applications of these materials. Here we report a mechanical strategy for creating certain classes of three-dimensional shapes in nanoribbons that would be difficult to generate in other ways. This approach involves the combined use of lithographically patterned surface chemistry to provide spatial control over adhesion sites, and elastic deformations of a supporting substrate to induce well-controlled local displacements. We show that precisely engineered buckling geometries can be created in nanoribbons of GaAs and Si in this manner and that these configurations can be described quantitatively with analytical models of the mechanics. As one application example, we show that some of these structures provide a route to electronics (and optoelectronics) with extremely high levels of stretchability (up to  $\sim 100\%$ ), compressibility (up to  $\sim 25\%$ ) and bendability (with curvature radius down to  $\sim 5$  mm).

Although various methods have been developed for defining the material composition<sup>1–6</sup>, diameter<sup>7–10</sup>, length<sup>11,12</sup> and position<sup>13–15</sup> of nanowires and nanoribbons, there are relatively few approaches for controlling their two- and three-dimensional (2D and 3D) configurations. Certain configurations can be controlled during growth to yield geometries such as coils<sup>16</sup>, rings<sup>17,18</sup> and branched layouts<sup>19,20</sup>, or after growth to produce, for example, sinusoidal wave-like structures by coupling these elements to strained elastomeric supports<sup>21</sup> or tube-like (or helical) structures by using built-in residual stresses in layered systems<sup>22,23</sup>. Semiconductor nanoribbons with wavy geometries are of interest in part because they enable the production of high-performance stretchable electronic systems for potential applications such as spherically curved focal plane arrays<sup>24</sup>, intelligent rubber surgical gloves<sup>25</sup> and conformable structural health monitors<sup>26</sup>. The approach for forming wavy geometries in semiconductor nanoribbons in which the electronic devices themselves are stretchable is different from and perhaps complementary to an alternative route to these same applications that uses rigid device islands with stretchable metal interconnects<sup>27</sup>. Previously described wavy nanoribbons have two main disadvantages<sup>21</sup>. First, they form spontaneously, with fixed periods and amplitudes defined by the moduli of the materials and the thicknesses of the ribbons, in a way that offers little control over the geometries or the phases of the waves. Second, the maximum strains that they can accommodate are in the range of 20–30%, limited by the non-optimal wavy geometries that result from this process. The procedures introduced here use lithographically defined surface adhesion sites together with elastic deformations of a supporting substrate to achieve buckling

configurations with deterministic control over their geometries. Periodic or aperiodic designs are possible, for any selected set of individual nanoribbons, in large-scale organized arrays of such structures. Specialized geometries designed for stretchable electronics enable strain ranges of up to nearly 150%, even in brittle materials such as GaAs, which is consistent with analytical modelling of the mechanics, and as much as ten times larger than previously reported results<sup>21</sup>.

## FABRICATION OF BUCKLES IN NANORIBBONS

Figure 1 shows the steps in the fabrication of buckles in nanoribbons. The fabrication starts with the preparation of a mask for patterning surface chemical adhesion sites on an elastomeric substrate of poly(dimethylsiloxane) (PDMS). This process involves passing deep ultraviolet (UV) light (240–260 nm) through an unusual type of amplitude photomask (fabricated in step i), referred to as a UVO mask<sup>28</sup>, while it is in conformal contact with the PDMS. The UVO mask possesses recessed features of relief in the transparent regions, such that exposure to UV light creates patterned areas of ozone proximal to the surface of the PDMS<sup>28</sup>. The ozone converts the unmodified hydrophobic surface, dominated by  $-\text{OSi}(\text{CH}_3)_2\text{O}-$  groups, to a highly polar and reactive surface (activated surface), terminated with  $-\text{O}_n\text{Si}(\text{OH})_{4-n}$  functionalities, which allow reactions with various inorganic surfaces to form strong chemical bonds<sup>29</sup>. The unexposed areas retain the unmodified surface chemistry (inactivated surface) and generate only weak van der Waals interactions with other surfaces<sup>30</sup>. The procedures introduced here

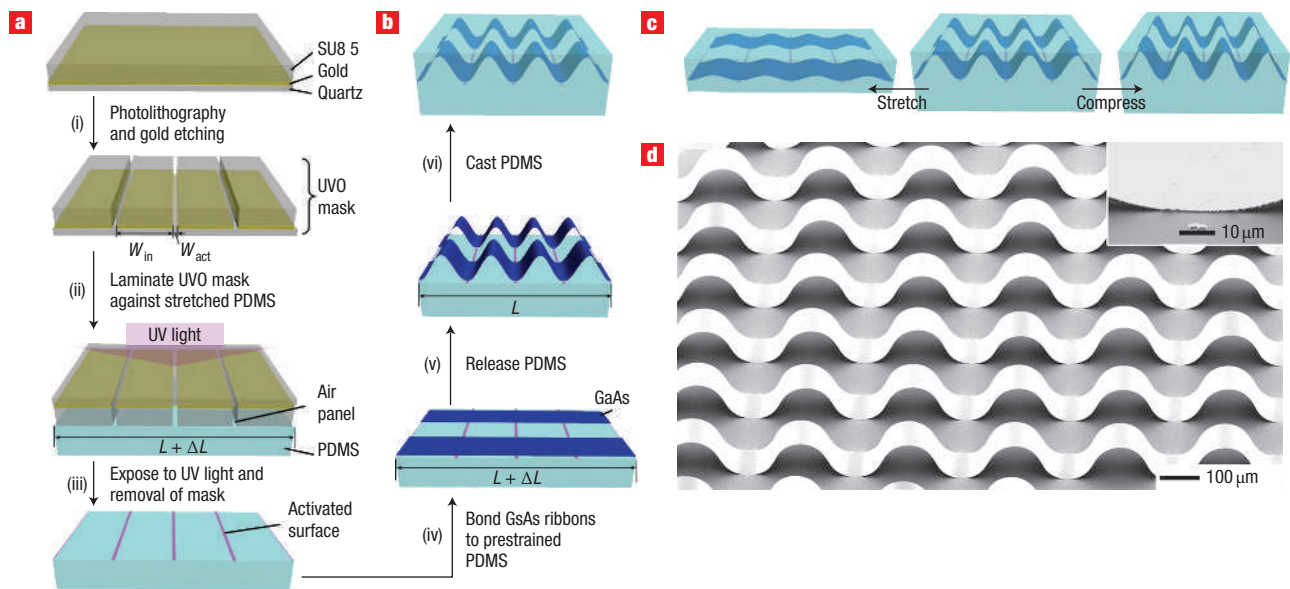


**Figure 1** Processing steps for engineering 3D buckled shapes in semiconductor nanoribbons. **a**, Fabrication of a UVO mask and its use in patterning the surface chemistry on a PDMS substrate. **b**, Formation of buckled GaAs ribbons and the process of embedding them in PDMS. **c**, Response of buckled GaAs ribbons to stretching and compressing. **d**, SEM image of a sample formed using the procedures in **a** and **b**. The pre-strain used for generating this sample was 60%, with  $W_{\text{act}} = 10 \mu\text{m}$  and  $W_{\text{in}} = 400 \mu\text{m}$ . (The inset shows an SEM image of a bonded region.)

involved exposures on PDMS substrates (thickness  $\sim 4 \text{ mm}$ ) under large, uniaxial prestrains ( $\varepsilon_{\text{pre}} = \Delta L/L$  for lengths changed from  $L$  to  $L + \Delta L$ ) (step ii). For masks with simple, periodic line patterns, we denote the widths of the activated (purple in the bottom frame of Fig. 1a) and inactivated stripes as  $W_{\text{act}}$  and  $W_{\text{in}}$  (step iii). The activated areas can bond strongly and irreversibly to other materials (for example, GaAs ribbons covered with  $\text{SiO}_2$  films and Si ribbons with native oxide layers) that have exposed  $-\text{Si}-\text{OH}$  groups on their surfaces due to the formation of strong siloxane linkages ( $-\text{O}-\text{Si}-\text{O}-$ ) through condensation reactions<sup>29,31</sup>. These patterned adhesion sites can be exploited to create well-defined 3D geometries in nanoribbons, as outlined in the following.

The nanoribbons consisted of both single-crystal Si and GaAs. The silicon ribbons were prepared from silicon-on-insulator (SOI) wafers using procedures described previously<sup>21</sup>. The GaAs ribbons involved multilayers of Si-doped  $n$ -type GaAs (120 nm; carrier concentration of  $4 \times 10^{17} \text{ cm}^{-3}$ ), semi-insulating GaAs (SI-GaAs; 150 nm) and AlAs (200 nm) formed on a (100) SI-GaAs wafer by molecular-beam epitaxy (MBE)<sup>32</sup>. Chemically etching the epilayers in an aqueous etchant of  $\text{H}_3\text{PO}_4$  and  $\text{H}_2\text{O}_2$  (ref. 31), using lines of photoresist patterned along the (011) crystalline orientation as etch masks, defined the ribbons. Removing the photoresist and then soaking the wafer in an ethanol solution of HF (2:1 volume ratio of ethanol and 49% aqueous HF) removed the AlAs layer, thereby releasing ribbons of GaAs ( $n$ -GaAs/SI-GaAs) with widths determined by the photoresist ( $\sim 100 \mu\text{m}$  for the examples shown here). The addition of ethanol to the HF solution reduced the probability of cracking of the fragile ribbons due to the action of capillary forces during drying. The low surface tension (compared to water) also minimized drying-induced disorder in the spatial layout of the GaAs ribbons. In the final step, a thin layer of  $\text{SiO}_2$  ( $\sim 30 \text{ nm}$ ) was deposited to provide the necessary  $-\text{Si}-\text{OH}$  surface chemistry for bonding to the activated regions of the PDMS.

By laminating the processed SOI or GaAs wafers against a UVO-treated prestretched PDMS substrate (ribbons oriented

parallel to the direction of pre-strain), baking in an oven at  $90^\circ \text{C}$  for 5 min, and removing the wafer, all of the ribbons were transferred to the surface of the PDMS (step iv). Heating facilitated conformal contact and the formation of strong siloxane linkages between the activated areas of the PDMS and the native  $\text{SiO}_2$  layer on the Si ribbons or the deposited  $\text{SiO}_2$  layer on the GaAs ribbons. Relatively weak van der Waals interactions bonded the ribbons to the inactivated regions of the PDMS. Relaxing the strain in the PDMS led to the formation of buckles through the physical separation of the ribbons from the inactivated regions of the PDMS (step v). The ribbons remained tethered to the PDMS in the activated regions owing to the strong chemical bonding. The resulting 3D ribbon geometries (that is, the spatially varying pattern of buckles) depend on the pre-strain and the patterns of surface activation. (Similar results can be achieved through patterned bonding sites on the ribbons). For the case of a simple line pattern,  $W_{\text{in}}$  and the pre-strain determine the width and amplitude of the buckles. Sinusoidal waves with wavelengths and amplitudes much smaller than the buckles also formed in the same ribbons when  $W_{\text{act}}$  was  $> 100 \mu\text{m}$ , owing to mechanical instabilities of the type that generate wavy silicon<sup>21</sup> (see Supplementary Information, Fig. S1, for images of samples formed with different values of  $W_{\text{act}}$ ). As a final step in the fabrication, the 3D ribbon structures can be encapsulated in PDMS by casting and curing a liquid prepolymer (step vi). Because of its low viscosity and low surface energy, the liquid flows and fills the gaps formed between the ribbons and the substrate (see Supplementary Information, Fig. S2).

Figure 1d shows a tilted-view scanning electron microscope (SEM) image of buckled GaAs ribbons on PDMS, in which  $\varepsilon_{\text{pre}} = 60\%$ ,  $W_{\text{act}} = 10 \mu\text{m}$  and  $W_{\text{in}} = 400 \mu\text{m}$ . The image reveals uniform, periodic buckles with common geometries and spatially coherent phases for all ribbons in the array. The anchoring points are well registered to the lithographically defined adhesion sites. The inset shows an SEM image of a bonded region; the width is

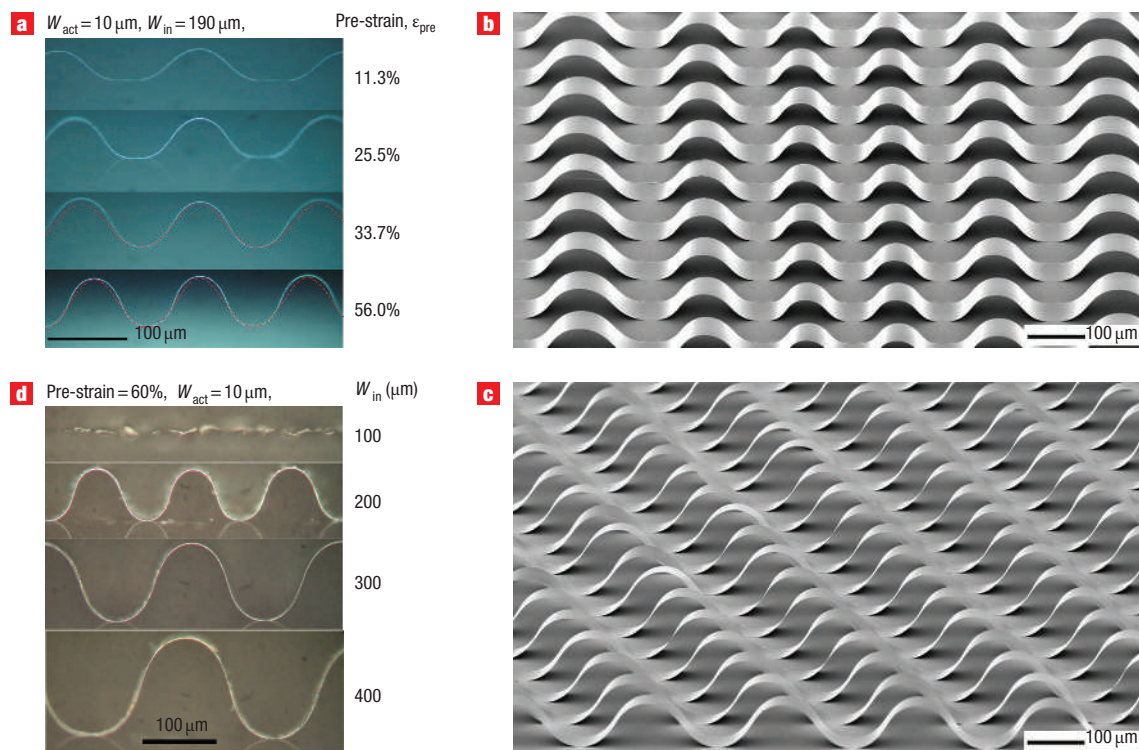


**Figure 2** Optical and SEM micrographs of the side-view profiles of buckled GaAs and Si ribbons. **a**, GaAs ribbon structures formed on PDMS substrates with different pre-strains,  $\epsilon_{\text{pre}}$ . **b**, Si ribbon structures formed on a PDMS substrate pre-strained to 50% and patterned with  $W_{\text{act}} = 15 \mu\text{m}$  and  $W_{\text{in}} = 350, 300, 250, 200, 150$  and  $100 \mu\text{m}$  (from left to right). The image was taken by tilting the sample at an angle of  $45^\circ$ . **c**, Si ribbon structures formed on a PDMS substrate pre-strained to 50% and patterned with parallel lines of adhesion sites ( $W_{\text{act}} = 15 \mu\text{m}$  and  $W_{\text{in}} = 250 \mu\text{m}$ ) oriented at angles of  $30^\circ$  with respect to the lengths of the ribbons. The image was taken by tilting the sample at an angle of  $75^\circ$ . **d**, GaAs ribbon structures formed on PDMS substrates patterned with different values of  $W_{\text{in}}$ .

$\sim 10 \mu\text{m}$ , consistent with  $W_{\text{act}}$ . The images also reveal that the surface of the PDMS is flat, even at the bonding sites. This behaviour, which is very different from the strongly coupled wavy structures reported previously<sup>21,33</sup>, suggests that the PDMS induces the displacements but is not intimately involved in the buckling process (that is, its modulus does not affect the geometries of the ribbons) for the cases described here. In this sense, the PDMS represents a soft, non-destructive tool for manipulating the ribbons through forces applied at the adhesion sites.

### STRETCHABILITY AND BENDABILITY OF BUCKLED NANORIBBONS

Figure 2a shows side-view optical micrographs of buckled ribbons formed on PDMS with different  $\epsilon_{\text{pre}}$  ( $W_{\text{act}} = 10 \mu\text{m}$  and  $W_{\text{in}} = 190 \mu\text{m}$ ). The heights of the buckles increase with  $\epsilon_{\text{pre}}$ . The ribbons in the inactivated regions do not fully separate at low  $\epsilon_{\text{pre}}$  (see the samples formed with  $\epsilon_{\text{pre}} = 11.3\%$  and  $25.5\%$ ). At higher  $\epsilon_{\text{pre}}$ , the ribbons (thickness  $h$ ) separate from the PDMS to form buckles with vertical displacement profiles characterized by  $y = (1/2)A_1^0(1 + \cos(\pi/L_1)x)$ , where  $A_1^0 = 4/\pi\sqrt{L_1L_2(\epsilon_{\text{pre}} - h^2\pi^2/12L_1^2)}$ , and  $L_1 = W_{\text{in}}/(2 \times (1 + \epsilon_{\text{pre}}))$ ,  $L_2 = L_1 + (W_{\text{act}}/2)$ , as determined by nonlinear analysis of buckles formed in a uniform thin layer (Jiang and co-workers, unpublished material). The maximum tensile strain in the ribbons is, approximately,  $\epsilon_{\text{peak}} = \kappa|_{\text{max}}(h/2) = y''|_{\text{max}}(h/2) = (h/4)A_1^0(\pi/L_1)^2$ . The width of the buckles is  $2L_1$  and the periodicity is  $2L_2$ . Because  $h^2\pi^2/12L_1^2$  is much smaller than  $\epsilon_{\text{pre}}$  for the cases investigated here, the amplitude is independent of the mechanical properties or thickness of ribbons

and is mainly determined by the layout of adhesion sites and the prestrain. This conclusion suggests a general applicability of this approach—ribbons made of any material will form into similar buckled geometries. This prediction is consistent with the results obtained with the Si and GaAs ribbons used here. The calculated profiles, plotted as dotted red lines in Fig. 2a for prestrains of  $33.7\%$  and  $56.0\%$ , agree well with the observations in GaAs ribbons. Further, the parameters (including periodicity, width and amplitude) of the buckles shown in Fig. 2a are consistent with analytical calculations, except at low  $\epsilon_{\text{pre}}$  (see Supplementary Information, Table S1). An interesting result of this study is that the maximum tensile strains in the ribbons are small (for example,  $\sim 1.2\%$ ), even for large  $\epsilon_{\text{pre}}$  (for example,  $56.0\%$ ). This scaling enables stretchability, even with brittle materials such as GaAs, as discussed subsequently.

The lithographically defined adhesion sites enable more complex geometries than the simple grating patterns associated with the structures in Fig. 1. For example, buckles with different widths and amplitudes can be formed in individual ribbons. Figure 2b shows, as an example, an SEM image of buckled Si ribbons (width  $50 \mu\text{m}$  and thickness  $290 \text{nm}$ ), formed with a pre-strain of  $50\%$  and adhesion sites characterized by  $W_{\text{act}} = 15 \mu\text{m}$  and  $W_{\text{in}} = 350, 300, 250, 200, 150$  and  $100 \mu\text{m}$  along the lengths of the ribbons. The image clearly shows the variation of widths and amplitudes of adjacent buckles in each of the ribbons. Buckled ribbons can also be formed with different phases for different ribbons. Figure 2c presents an example of a Si system designed with phases in the buckles that vary linearly with distance perpendicular to the lengths of the ribbons. The

UVO mask used for this sample has  $W_{\text{act}}$  and  $W_{\text{in}}$  of 15 and 250  $\mu\text{m}$ , respectively. The angle between the activated stripes on PDMS stamp and Si ribbons is  $30^\circ$ . Many other possibilities can easily be achieved, with simple lithographic control of the adhesion sites.

The simple case of buckled GaAs ribbons on PDMS with  $\varepsilon_{\text{pre}} = 60\%$ ,  $W_{\text{act}} = 10 \mu\text{m}$  and different values of  $W_{\text{in}}$ , as shown in Fig. 2d, illustrates an aspect that is important for applications in stretchable electronics. The profiles, which agree well with analytical solutions to the mechanics, show failure due to cracking in the GaAs when  $W_{\text{in}} = 100 \mu\text{m}$  (and smaller). The failure results from tensile strains ( $\sim 2.5\%$  in this case) that exceed the yield point of the GaAs ( $\sim 2\%$ ). An optimized configuration for robustness to stretching and compressing can, therefore, be achieved by selecting  $W_{\text{in}} \gg W_{\text{act}}$ . In this situation, pre-strains up to and greater than 100% can be accommodated. The only limit is in the resolution with which we can pattern the adhesion sites on the PDMS, which is  $\sim 2 \mu\text{m}$ , with current approaches. We demonstrated this type of stretchability directly by applying forces to the PDMS supports. Changes in the end-to-end distances ( $L_{\text{projected}}$ ) of segments of the ribbons provided a means to quantify the stretchability and compressibility, according to  $|(L_{\text{projected}}^* - L_{\text{projected}}^0)/L_{\text{projected}}^0| \times 100\%$ , where  $L_{\text{projected}}^*$  represents the maximum or minimum length before fracture and  $L_{\text{projected}}^0$  is the length in the relaxed state. Stretching and compressing correspond to  $L_{\text{projected}}^*$  greater and less than  $L_{\text{projected}}^0$ , respectively. Buckled ribbons on PDMS with  $W_{\text{act}} = 10 \mu\text{m}$  and  $W_{\text{in}} = 400 \mu\text{m}$  and  $\varepsilon_{\text{pre}} = 60\%$ , exhibit stretchability of 60% (that is,  $\varepsilon_{\text{pre}}$ ) and compressibility of up to 30%. Embedding the ribbons in PDMS mechanically protects the structures, and also produces a continuous, reversible response, but with slightly different mechanics compared to the unembedded case. In particular, the stretchability and compressibility decreased to  $\sim 51.4\%$  (Fig. 3a) and  $\sim 18.7\%$  (Fig. 3b), respectively. The PDMS matrix on top of the ribbons flattens the peaks of the buckles slightly, owing partly to curing-induced shrinkage of the overlying PDMS. Small period waves form in these regions under large compressive strains, due to the spontaneous mechanics of the type that generated the wavy ribbon structures described previously<sup>21</sup>. Mechanical failure tends to initiate in these areas, as illustrated in Fig. 3b, thereby reducing the compressibility. Buckled structures with  $W_{\text{act}} = 10 \mu\text{m}$  and  $W_{\text{in}} = 300 \mu\text{m}$  avoided this type of behaviour. Although such samples exhibited slightly lower stretchability than the one shown in Fig. 3a, the absence of the short period waves increased the compressibility to  $\sim 26\%$ . Overall, single-crystalline GaAs nanoribbons with buckles that were formed on the prestretched PDMS substrates with patterned surface chemical adhesion sites exhibit stretchability higher than 50%, and compressibility larger than 25%, corresponding to full-scale strain ranges approaching 100%. These numbers can be further improved by increasing  $\varepsilon_{\text{pre}}$  and  $W_{\text{in}}$ , and by using a substrate material capable of higher elongation than PDMS. For even more elaborate systems, these fabrication procedures can be repeated to generate 3D multilayered architectures (see Supplementary Information, Fig. S3).

A direct consequence of this large stretchability and compressibility is extreme levels of mechanical bendability. Figure 4a–c presents optical micrographs of bent configurations that illustrate this feature. The PDMS substrate (thickness  $\sim 4 \text{ mm}$ ) was bent into concave (radius  $\sim 5.7 \text{ mm}$ ), flat and convex (radius  $\sim 6.1 \text{ mm}$ ) curvatures, respectively. The images illustrate how the profiles changed to accommodate the bending induced surface strains ( $\sim 20\text{--}25\%$  for these cases). The shapes are similar, in fact, to those obtained in compression (by strains of  $\sim 20\%$ ) and tension (by strains of  $\sim 20\%$ ). The

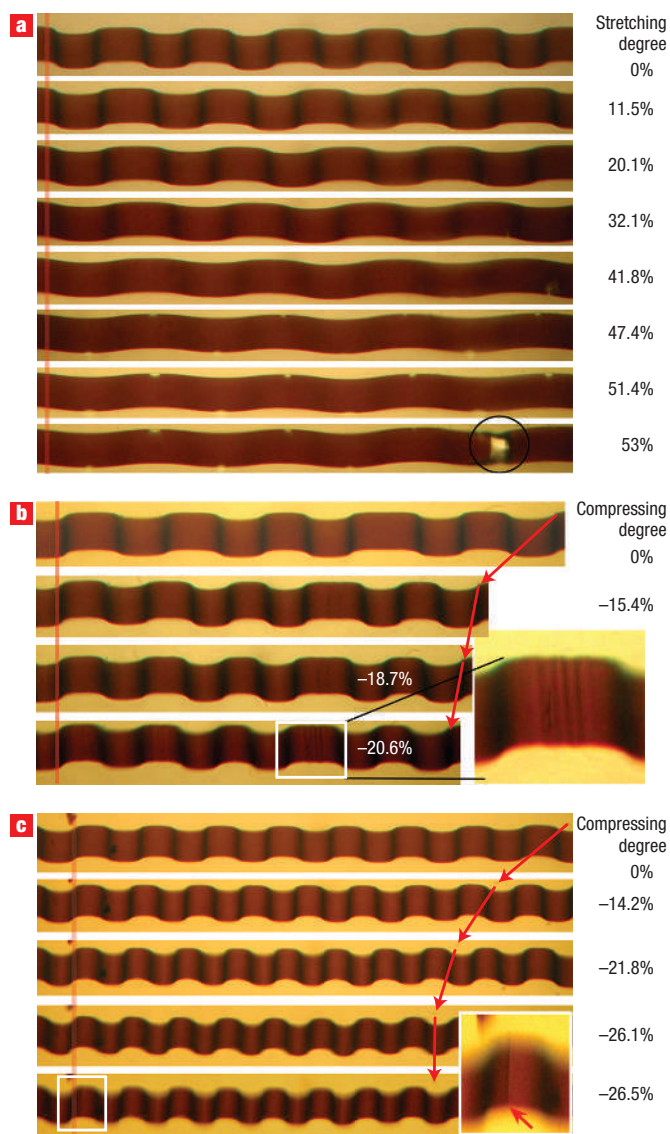


**Figure 3** Stretching and compressing of buckled GaAs ribbons embedded in PDMS. **a**, Images of a single buckled ribbon stretched to different levels of tensile strain (positive %). Fracture occurs near 50%. **b**, Images of a single buckled ribbon compressed to different levels of compressive strain (negative %). Small, short-period wavy geometries appear at the peaks of the buckles for compressive strains larger than  $\sim 15\%$ . **c**, Images of a single buckled ribbon compressed to different levels of compressive strain. The buckles in these cases were formed with a pre-strain of 60% with  $W_{\text{act}} = 10 \mu\text{m}$  and  $W_{\text{in}} = 400 \mu\text{m}$  (**a,b**) and with  $W_{\text{act}} = 10 \mu\text{m}$  and  $W_{\text{in}} = 300 \mu\text{m}$  (**c**). The red lines and arrows in each panel indicate the same positions on the same ribbons to highlight the mechanical deformations. The insets provide magnified images of the sections marked with the white boxes, clearly showing the formation of cracks at high compressive strains. The numbers corresponding to stretching or compressing degree were computed according to  $[(L_{\text{projected}} - L_{\text{projected}}^0)/L_{\text{projected}}^0] \times 100\%$ .

embedded systems exhibited even higher levels of bendability due to neutral mechanical plane effects<sup>34,35</sup>. When the top and bottom layers of PDMS had similar thicknesses, there was no change in the buckling shapes during bending (Fig. 4d).

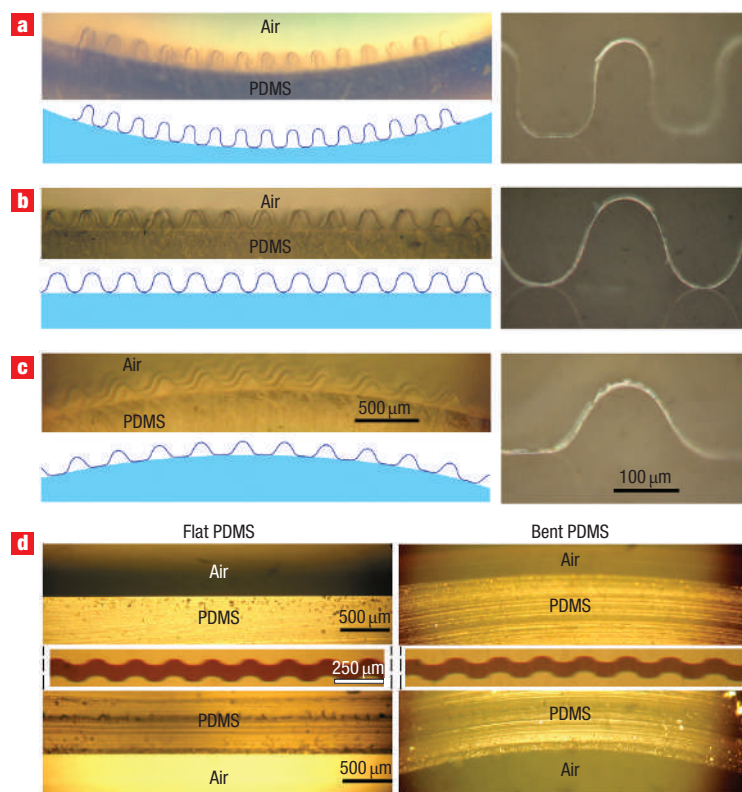


**Figure 4** Bending of buckled ribbons on surfaces and in matrixes of PDMS. **a–c**, Optical microscope images with low magnification (top left frames) and high magnification (right frames) and schematic illustrations (bottom left frames) of buckled GaAs ribbons on PDMS with concave (**a**), flat (**b**) and convex (**c**) surfaces. (The scale bars in panel **c** also apply to panels **a** and **b**.) **d**, Images of buckled ribbons embedded in PDMS before (left) and after (right) bending. A single embedded GaAs ribbon can be seen in the enlarged area enclosed in the white box. The top and bottom frames show the curvatures of the top and bottom surfaces, respectively. The buckled ribbons are the same as those shown in Fig. 1d.

### STRETCHABLE ELECTRONICS WITH BUCKLED NANORIBBONS

To demonstrate these mechanical properties in functional electronic devices, we built metal–semiconductor–metal photodetectors (MSM PDs) using buckled GaAs ribbons with profiles similar to those shown in Fig. 4, by depositing thin gold electrodes onto the Si–GaAs sides of the ribbons to form Schottky contacts. Figure 5a shows the geometry and equivalent circuit, and top-view optical micrographs of an MSM PD before and after stretching by  $\sim 50\%$ . In the absence of light, little current flowed through the PD; the current increased with an increase of illumination with an infrared beam (wavelength  $\sim 850$  nm) (Fig. 5b). The asymmetry in the current/voltage ( $I$ – $V$ ) characteristics can be attributed to differences in the electrical properties of the contacts. Figure 5c (stretching) and 5d (compressing) show  $I$ – $V$  characteristics measured at different degrees of stretching and compressing. The current increased when the PD was stretched by up to 44.4% and then decreased with further stretching. Because the intensity per unit area of the light source is constant, the increases in current with stretching can be attributed to increases in the projected area (referred to as effective area,  $S_{\text{eff}}$ ) of the buckled GaAs ribbon as it flattens. Further stretching of the PD might induce the formation of defects on the surface and/or in the lattice of the GaAs ribbon, resulting in a decrease of current and, eventually, at fracture, in an open circuit. Similarly, compression led to a decrease in  $S_{\text{eff}}$  and also a decrease in the current (Fig. 5d). These results indicate that buckled GaAs ribbons embedded in a PDMS matrix provide a fully stretchable/compressible type of photosensor that could be useful

in various applications, such as wearable monitors, curved imaging arrays and other devices.

In conclusion, the results presented here indicate that soft elastomers with lithographically defined adhesion sites can be used as tools for creating certain classes of 3D configurations in semiconductor nanoribbons. Stretchable electronics provide one example of the many possible application areas for these types of structures. Simple PD devices demonstrate some of these capabilities. The high level of control over the structures and the ability to separate high-temperature processing steps (such as formation of ohmic contacts) from the buckling process and the PDMS suggest that more complex devices (for example, transistors and small circuit sheets) are possible. The well-controlled phases of buckles in adjacent ribbons provide an opportunity for electrically interconnecting multiple elements. Also, although the experiments reported here used GaAs and Si nanoribbons, other materials, such as GaN and InP, and other structures, such as nanowires and nanomembranes, should also be compatible with this approach.

### METHODS

#### FABRICATION OF GaAs RIBBONS

Photolithography and wet chemical etching was used to generate GaAs ribbons from GaAs wafers with customer-designed epitaxial layers (IQE). An AZ 5214 photoresist was spin-cast on the GaAs wafers (5,000 r.p.m., 30 s) and then baked at 100 °C for 1 min. Exposure through a photomask with patterned lines oriented along the (011) crystallographic direction of GaAs, followed by

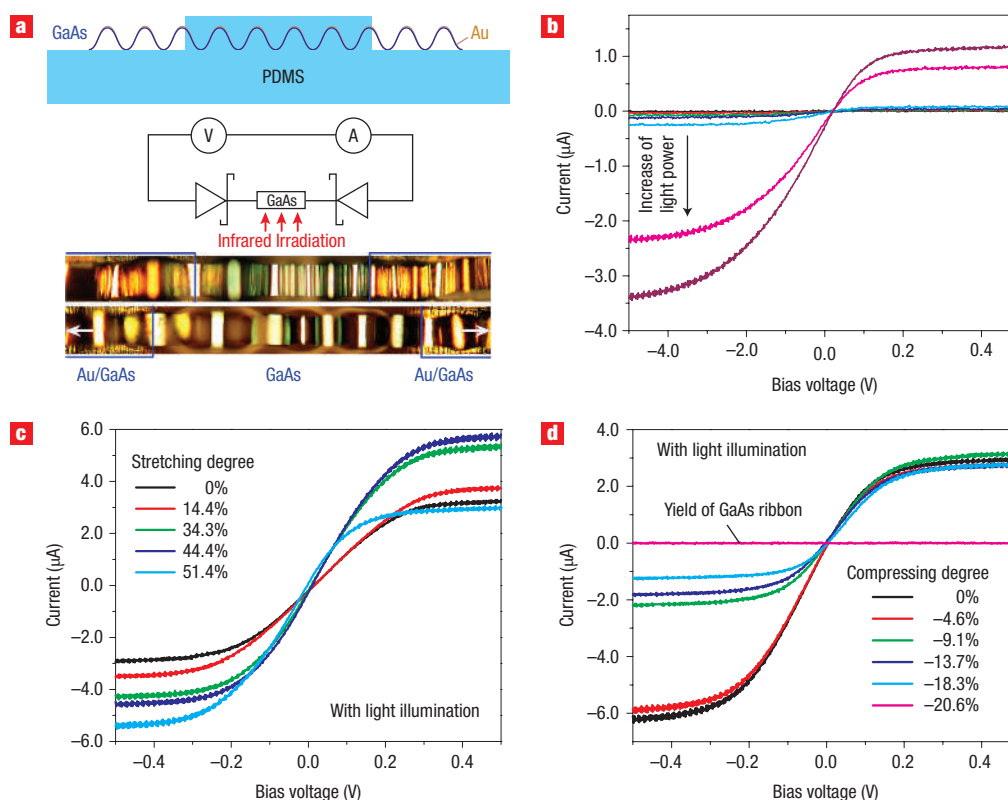


**Figure 5** Characterization of stretchable metal–semiconductor–metal photodetectors (MSM PDs). **a**, Schematic illustrations of the geometry (top), an equivalent circuit (middle) and optical images of a buckled PD before and during stretching (bottom, the white arrows indicate the direction of force applied during stretching). **b**, Current/voltage ( $I$ – $V$ ) curves recorded from a buckled PD that was irradiated by an Infrared lamp with different output intensities. **c,d**,  $I$ – $V$  characteristics of PDs illuminated with constant luminance and stretched (**c**) or compressed (**d**) to different degrees.

development, generated line patterns in the photoresist. Mild  $O_2$  plasma removed the residual photoresist. The GaAs wafers were then etched for 1 min in the etchant (4 ml  $H_3PO_4$  (85 wt%), 52 ml  $H_2O_2$  (30 wt%) and 48 ml deionized water), which was cooled in the ice-water bath. The AlAs layers were dissolved with an HF solution diluted in ethanol (1:2 in volume). The samples with released ribbons on mother wafers were dried in a fume hood. The dried samples were coated with 30-nm  $SiO_2$  deposited by electron beam evaporation.

#### FABRICATION OF Si RIBBONS

Si ribbons were fabricated from SOI wafers (Soitec top silicon 290 nm, buried oxide 400 nm). The wafers were patterned by conventional photolithography using AZ 5214 photoresist and etched with  $SF_6$  plasma. After the photoresist was washed away with acetone, the buried oxide layer was then etched in HF (49%).

#### FABRICATION OF UVO MASKS

Fused quartz slides were cleaned in piranha solution (at 60 °C) for 15 min and thoroughly rinsed with plenty of water. The dry, cleaned slides were coated with sequential layers of 5-nm Ti (adhesive layers) and 100-nm Au (mask layers for UV light) by electron-beam evaporation. A negative photoresist (SU8 5) was spin-cast on the slides (3,000 r.p.m., 30 s) to yield  $\sim 5$ - $\mu$ m-thick films. Patterns were generated in the photoresist by soft baking, exposure to UV light, post baking and developing. Mild  $O_2$  plasma removed the residual photoresist. The photoresist served as a mask to etch Au and Ti using gold etchant (aqueous solution of  $I_2$  and KI) and titanium etchant (diluted solution of HCl), respectively.

#### PREPARATION OF PDMS STAMPS

PDMS substrates of thickness  $\sim 4$  mm were prepared by pouring the prepolymer 1:10, Sylgard 184, Dow Corning into a Petri dish and baking at 65 °C for 4 h. Rectangular Slabs of suitable sizes were cut from the resulting cured piece, then rinsed with isopropyl alcohol and dried using nitrogen

blowing. A specially designed stage was used to mechanically stretch the PDMS to the desired levels of strain. Illuminating these stretched substrates with short-wavelength UV light (low-pressure mercury lamp,  $173 \mu W cm^{-2}$  from 240 to 260 nm, BHK) for 5 min through a UVO mask placed in contact with the PDMS generated the patterned surface chemistries.

#### FORMATION AND EMBEDDING OF BUCKLED GaAs (OR Si) RIBBONS

GaAs wafers with released ribbons coated with  $SiO_2$  (or Si ribbons with native oxide layer) were laminated against the stretched PDMS with patterned surface chemistry. Baking in an oven at 90 °C for 5 min, cooling to room temperature in air, and then slowly relaxing the strain in the PDMS generated buckles along each ribbon. Embedding the buckled ribbons involved flood exposure to UV light for 5 min followed by the casting of liquid PDMS prepolymers to a thickness of  $\sim 4$  mm. Leaving the sample either in an oven at 65 °C for 4 h or at room temperature for 36 h cured the prepolymer, to leave the buckled ribbons embedded in a solid matrix of PDMS.

#### CHARACTERIZATION OF BUCKLED RIBBONS

The ribbons were imaged with an optical microscope by tilting the sample by  $\sim 90^\circ$  (for non-embedded samples) or  $\sim 30^\circ$  (for embedded samples). The SEM images were recorded on a Philips XL30 field-emission scanning electron microscope after the sample was coated with a thin layer of gold ( $\sim 5$  nm in thickness). The same stage used for pre-stretching the PDMS stamps was used to stretch and compress the resulting samples.

#### FABRICATION AND CHARACTERIZATION OF MSM PDs

Fabrication of PDs started with samples in the configuration shown in the bottom frame of Fig. 1b. An  $\sim 0.8$ -mm-wide strip of poly(ethylene terephthalate) (PET) sheet was gently placed on the PDMS with its longitudinal axis perpendicular to the longitudinal axes of the ribbons. This strip served as a shadow mask for electron-beam evaporation of a 30-nm-thick gold film (to form Schottky electrodes). Removing the PET strip, and relaxing the

prestretched PDMS stamp resulted in MSM PDs built with buckled GaAs ribbons. Liquid PDMS prepolymer was cast onto the regions of the ribbons without electrodes and then cured in an oven. The gold electrodes extended beyond the top PDMS to enable probing with a semiconductor parameter analyser (Agilent 4155C). In measurements of the photoresponse, the PDs were manipulated using a mechanical stage for stretching and compressing. An infrared LED source (with wavelength 850 nm) provided the illumination.

Received 14 August 2006; accepted 28 September 2006; published 5 December 2006.

## References

- Duan, X. & Lieber, C. M. General synthesis of compound semiconductor nanowires. *Adv. Mater.* **12**, 298–302 (2000).
- Xiang, J. *et al.* Ge/Si nanowire heterostructures as high-performance field-effect transistors. *Nature* **441**, 489–493 (2006).
- Wu, Y. *et al.* Inorganic semiconductor nanowires: rational growth, assembly, and novel properties. *Chem. Eur. J.* **8**, 1261–1268 (2002).
- Pan, Z. W., Dai, Z. R. & Wang, Z. L. Nanobelts of semiconducting oxides. *Science* **291**, 1947–1949 (2001).
- Peng, X. *et al.* Shape control of CdSe nanocrystals. *Nature* **404**, 59–61 (2000).
- Wang, D., Chang, Y.-L., Lu, Z. & Dai, H. Oxidation resistant germanium nanowires: bulk synthesis, long chain alkanethiol functionalization, and Langmuir–Blodgett assembly. *J. Am. Chem. Soc.* **127**, 11871–11875 (2005).
- Huang, M. H. *et al.* Catalytic growth of zinc oxide nanowires by vapor transport. *Adv. Mater.* **13**, 113–116 (2001).
- Gudiksen, M. S., Wang, J. & Lieber, C. M. Synthetic control of the diameter and length of single crystal semiconductor nanowires. *J. Phys. Chem. B* **105**, 4062–4064 (2001).
- Yu, H., Li, J., Loomis, R. A., Wang, L.-W. & Buhro, W. E. Two- versus three-dimensional quantum confinement in indium phosphide wires and dots. *Nature Mater.* **2**, 517–520 (2003).
- Sun, Y. *et al.* Photolithographic route to the fabrication of micro/nanowires of III-V semiconductors. *Adv. Funct. Mater.* **15**, 30–40 (2005).
- Yin, Y., Gates, B. & Xia, Y. A soft lithography approach to the fabrication of nanostructures of single crystalline silicon with well-defined dimensions and shapes. *Adv. Mater.* **12**, 1426–1430 (2000).
- Kodambaka, S., Hannon, J. B., Tromp, R. M. & Ross, F. M. Control of Si nanowire growth by oxygen. *Nano Lett.* **6**, 1292–1296 (2006).
- Shan, Y., Kalkan, A. K., Peng, C.-Y. & Fonash, S. J. From Si source gas directly to positioned, electrically contacted Si nanowires: the self-assembling “grow-in-place” approach. *Nano Lett.* **4**, 2085–2089 (2004).
- He, R. *et al.* Si nanowire bridges in microtrenches: integration of growth into device fabrication. *Adv. Mater.* **17**, 2098–2102 (2005).
- Lee, K. J. *et al.* Large-area, selective transfer of microstructured silicon: a printing-based approach to high-performance thin-film transistors supported on flexible substrates. *Adv. Mater.* **17**, 2332–2336 (2005).
- Gao, P. X. *et al.* Conversion of zinc oxide nanobelts into superlattice-structured nanohelices. *Science* **309**, 1700–1704 (2005).
- Kong, X. Y., Ding, Y., Yang, R. & Wang, Z. L. Single-crystal nanorings formed by epitaxial self-coiling of polar nanobelts. *Science* **303**, 1348–1351 (2004).
- Chen, P., Chua, S. J., Wang, Y. D., Sander, M. D. & Fonstad, C. G. InGaN nanorings and nanodots by selective area epitaxy. *Appl. Phys. Lett.* **87**, 143111 (2005).
- Manna, L., Milliron, D. J., Meisel, A., Scher, E. C. & Alivisatos, A. P. Controlled growth of tetrapod-branched inorganic nanocrystals. *Nature Mater.* **2**, 382–385 (2003).
- Dick, K. A. *et al.* Synthesis of branched ‘nanotrees’ by controlled seeding of multiple branching events. *Nature Mater.* **3**, 380–384 (2004).
- Khang, D.-Y., Jiang, H., Huang, Y. & Rogers, J. A. A stretchable form of single-crystal silicon for high-performance electronics on rubber substrates. *Science* **311**, 208–212 (2006).
- Schmidt, O. G. & Eberl, K. Thin solid films roll up into nanotubes. *Nature* **410**, 168–168 (2001).
- Zhang, L. *et al.* Anomalous coiling of SiGe/Si and SiGe/Si/Cr helical nanobelts. *Nano Lett.* **6**, 1311–1317 (2006).
- Jin, H.-C., Abelson, J. R., Erhardt, M. K. & Nuzzo, R. G. Soft lithographic fabrication of an image sensor array on a curved substrate. *J. Vac. Sci. Technol. B* **22**, 2548–2551 (2004).
- Someya, T. *et al.* A large-area, flexible pressure sensor matrix with organic field-effect transistors for artificial skin applications. *Proc. Natl Acad. Sci. USA* **101**, 9966–9970 (2004).
- Nathan, A. *et al.* Amorphous silicon detector and thin film transistor technology for large-area imaging of X-rays. *Microelectronics J.* **31**, 883–891 (2000).
- Lacour, S. P., Jones, J., Wagner, S., Li, T. & Suo, Z. Stretchable interconnects for elastic electronic surfaces. *Proc. IEEE* **93**, 1459–1467 (2005).
- Childs, W. R., Motala, M. J., Lee, K. J. & Nuzzo, R. G. Masterless soft lithography: patterning UV/Ozone-induced adhesion on poly (dimethylsiloxane) surfaces. *Langmuir* **21**, 10096–10105 (2005).
- Duffy, D. C., McDonald, J. C., Schueller, O. J. A. & Whitesides, G. M. Rapid prototyping of microfluidic systems in poly (dimethylsiloxane). *Anal. Chem.* **70**, 4974–4984 (1998).
- Huang, Y. Y. *et al.* Stamp collapse in soft lithography. *Langmuir* **21**, 8058–8068 (2005).
- Sun, Y. & Rogers, J. A. Fabricating semiconductor nano/microwires and transfer printing ordered arrays of them onto plastic substrates. *Nano Lett.* **4**, 1953–1959 (2004).
- Sun, Y., Kumar, V., Adesida, I. & Rogers, J. A. Buckled and wavy ribbons of GaAs for high-performance electronics on elastomeric substrates. *Adv. Mater.* **18**, 2857–2862 (2006).
- Bowden, N., Brittain, S., Evans, A. G., Hutchinson, J. W. & Whitesides, G. M. Spontaneous formation of ordered structures in thin films of metals supported on an elastomeric polymer. *Nature* **393**, 146–149 (1998).
- Loo, Y.-L. *et al.* Soft, conformable electrical contacts for organic semiconductors: high-resolution plastic circuits by lamination. *Proc. Natl Acad. Sci. U.S.A.* **99**, 10252–10256 (2002).
- Suo, Z., Ma, E. Y., Gleskova, H. & Wagner, S. Mechanics of rollable and foldable film-on-foil electronics. *Appl. Phys. Lett.* **74**, 1177–1179 (1999).

## Acknowledgements

This work was supported by the U.S. Department of Energy under grant DEFG02-91-ER45439. The fabrication and measurements were carried out using the facilities located in the Microfabrication Laboratory of Frederick Seitz Materials Research Laboratory, which are supported by the Department of Energy. W.M. Choi would like to acknowledge the financial support from Korea Research Foundation grant KRF-2005-214-D00261, funded by the Korean Government (MOEHRD). Argonne National Laboratory’s work (partially for Y. Sun) was supported by the U.S. Department of Energy, Office of Science, Office of Basic Energy Sciences, under contract DE-AC-02-06CH11357. Correspondence and requests for materials should be addressed to J.A.R. Supplementary Information accompanies this paper on [www.nature.com/naturenanotechnology](http://www.nature.com/naturenanotechnology).

## Author contributions

Y.S. and J.A.R. conceived and designed the experiments, Y.S. and W.M.C. performed the experiments, and H.J. and Y.Y.H. modelled the mechanical behaviour of the samples. Y.S. and J.A.R. co-wrote the paper.

## Competing financial interests

The authors declare that they have no competing financial interests.

Reprints and permission information is available online at <http://npg.nature.com/reprintsandpermissions/>